Excitation of the modified Simon–Hoh instability in an electron beam produced plasma

Y. Sakawa, C. Joshi, P. K. Kaw,[a] F. F. Chen, and V. K. Jain[b]
Department of Electrical Engineering, University of California, Los Angeles, California 90024

(Received 13 May 1992; accepted 13 January 1993)

An intermediate frequency ($f_{ci} < f < f_{ce}$) electrostatic instability has been observed in an electron beam produced, cylindrical plasma column. This instability has been identified as a new instability, the modified Simon–Hoh instability (MSHI), which has an instability mechanism similar to the Simon–Hoh instability (SHI). This instability can occur in a cylindrical collisionless plasma if a radial dc electric field exists and if this radial dc electric field and the radial density gradient are in the same direction. The origin of the dc electric field is found to be the difference between the ion and the electron radial density profiles. In such a plasma if the ions are essentially unmagnetized but the electrons are magnetized, a velocity difference in the θ direction can arise because of the finite ion Larmor radius effect. This leads to a space charge separation between the electron and ion density perturbations in the θ direction. The consequent perturbed azimuthal electric field $E_{\theta 1}$ and the enhancement of the density perturbation by the $E_{\theta 1} \times B_0$ velocity occur in the same manner as in the SHI. The instability frequency is decided by the ion azimuthal drift velocity. This new instability has been investigated through experiments and theory.

I. INTRODUCTION

Intermediate frequency electrostatic instabilities driven by the relative drift of electrons and ions across an external magnetic field have been studied by many authors.[1–5] By intermediate frequency we mean $f_{ci} \ll f \ll f_{ce}$, where f_{ci} and f_{ce} are ion and electron cyclotron frequencies, respectively. Simon[6] and Hoh[7] studied the Simon–Hoh instability (SHI) in a weakly ionized, inhomogeneous, collisional, magnetized plasma under a strong electric field perpendicular to the dc magnetic field. The SHI is unstable when the density gradient and the electric field are in the same direction, and is triggered by the difference between the electron and ion $E \times B$ drift velocities caused by collisions. The SHI was observed by Thomassen[8] in a hot cathode Penning discharge plasma. In collisionless, weakly magnetized-ion plasmas (where electrons are magnetized), a similar instability may be expected due to the slower (relative to the electron) ion drift velocity caused by the large ion Larmor radius effect.

In this paper, we report the observation and identification of such a new intermediate frequency electrostatic instability in an electron beam produced plasma which we call the modified Simon–Hoh instability (MSHI). The instability mechanism of the MSHI is best explained by first briefly explaining the SHI and then by pointing out the crucial differences between the two. SHI is an instability in a weakly ionized, collisional ($\omega \ll \nu_{en}, \nu_{in}$) plasma with an axial magnetic field and a radial dc electric field. Here ν_{en} and ν_{in} are the electron–neutral elastic collision and ion–neutral charge exchange collision frequencies, respectively. (See Table I for explanation of various symbols and their typical values in our experiment which will be described later.) SHI occurs when both ions and electrons are magnetized, the density is nonuniform ($\nabla n_0 \neq 0$) in the direction of the electric field (E_{r0}), and when the sign of the product of the electric field and the density gradient is positive ($\nabla n_0 \cdot \mathbf{E}_{r0} > 0$). The instability mechanism of SHI is as follows: Under the dc axial B_0 field and the radial E_{r0} field, both electrons and ions rotate with $E_{r0} \times B_0$ drift velocity,

$$v_{Ej} = \frac{E_{r0}/B}{1 + (1/\Omega_j^2 \tau_{jn}^2)}, \tag{1}$$

where $j = e$ (electron) or i (ion), Ω_j is the cyclotron frequency and τ_{jn} is the collision time with the neutral gas. Since $\Omega_e^2 \tau_{en}^2 \gg 1$ and $\Omega_i^2 \tau_{in}^2 \gg 1$, we obtain

$$v_{Ee} = E_{r0}/B, \tag{2}$$

whereas

$$v_{Ei} = \frac{E_{r0}/B}{1 + (1/\Omega_i^2 \tau_{in}^2)}. \tag{3}$$

This difference between the electron and ion $E \times B$ drift velocities causes a space charge separation between the electron and ion density perturbations in the θ direction,

[a] Present address: Institute for Plasma Research, Bhat, Gandhinagar 382 424, India.
[b] Present address: School of Environmental Science, Jawaharlal Nehru University, New Delhi 110 067, India.

 0899-8221/93/061681-14$06.00

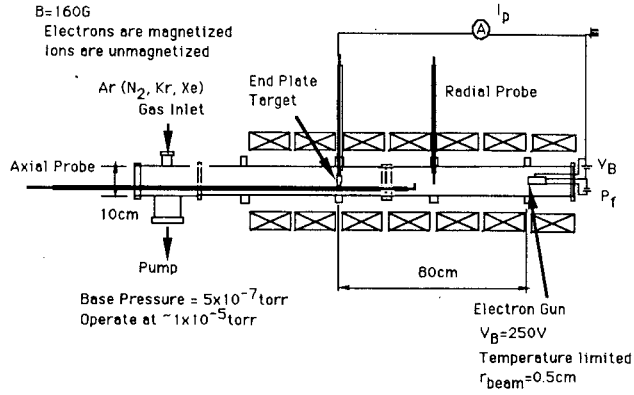

FIG. 1. The experimental setup of the beam–plasma system. The plasma is produced by collisional ionization of the neutral gas by the electron beam.

and consequently produces a perturbed azimuthal electric field, $E_{\theta 1}$. When the plasma density is inhomogeneous and $\nabla n_0 \cdot \mathbf{E}_{r0} > 0$, then the $E_{\theta 1} \times B_0$ velocity enhances the density perturbation. The instability frequency of SHI is roughly $v_{Ec} k_\theta$.

The instability considered in this paper, MSHI, is different from the collisional SHI in that, (a) ions are unmagnetized and (b) both electrons and ions are collisionless. Therefore, the azimuthal velocity of the ions is not expressed by Eq. (3). Here, the velocity difference between electrons and ions is caused by the large ion Larmor radius effect. In our experiment, the ions are unmagnetized because of the small axial B field. Furthermore, because of the large dc radial electric field they move radially in and out across the B field. Therefore, the ion orbit is nearly a straight line. As the ions pass the vicinity of the center of the plasma, they are pushed outwards due to the $v \times B$ force. Even though this perturbation of the ion orbit from a straight line is small, its curvature cannot be neglected. Upon averaging over many ions, the ions are always seen to pass the center in the direction of the $E_{r0} \times B_0$ drift. This ion azimuthal drift velocity can be much smaller than the electron $E_{r0} \times B_0$ velocity and therefore causes a space charge separation between the electron and ion density perturbations in the θ direction. The consequent perturbed azimuthal electric field $E_{\theta 1}$ and the enhancement of the density perturbation by the $E_{\theta 1} \times B_0$ velocity are the same as in the SHI case.

This paper is organized as follows: Sec. II describes the experimental apparatus and measurements; in Sec. III the theory of the MSHI is given and a comparison of the MSHI with other instabilities is made; in Sec. IV experimental results are compared with the theory; the conclusion and a summary of the paper are given in Sec. V.

II. EXPERIMENTS

Figure 1 shows the experimental setup of our beam-plasma system used in this work. A 1 cm full width at half-maximum (FWHM) diameter Gaussian electron beam is injected axially into one end of a 10 cm diameter,

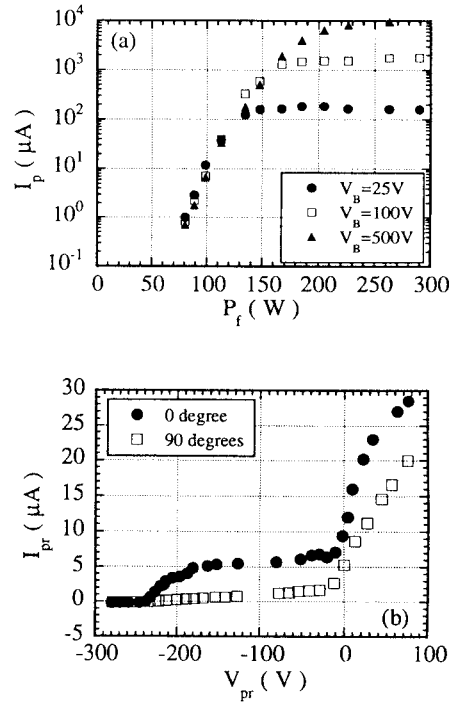

FIG. 2. Electron gun and probe characteristics. (a) Dependence of the electron current collected at the grounded endplate I_p on the filament heating power P_f. I_p is governed by temperature limited emission at lower P_f, and governed by space-charge limited emission at higher P_f. Experiments were performed at $V_B = 250$ V, $I_p = 10$ to 1000 μA, which is in the temperature limited emission region. (b) Probe characteristics measured by a 2×2 mm square disk probe (0.05 mm in thickness). The beam acceleration voltage V_B is 250 V in this measurement. For the probe bias voltage $V_{pr} < -250$ V, only the ion saturation current is collected; for $V_{pr} > 0$ V, the contribution is mainly from the plasma electrons; a clear beam electron component is observed for $-250\ \text{V} < V_{pr} < 0$ V when the disk is normal to the electron beam (closed circle); when the disk is parallel to the electron beam (open square), a very small beam component collected by the edge area of 0.05 mm thickness$\times$2 mm length is observed.

180 cm long stainless steel vacuum vessel, immersed in a dc magnetic field of up to 320 G. Most of our measurements are conducted at $B = 160$ G. The distance between the electron gun and a grounded endplate target (1.2 cm diam) defines the interaction length to be 80 cm. The magnetic field uniformity over the interaction region is better than 3%. For most of our measurements, which are carried out over the pressure range 5×10^{-6} to 5×10^{-5} Torr, Ar gas is used. The vacuum base pressure is $\simeq 5\times10^{-7}$ Torr. The ion mass dependence of the observed instability is determined by using Xe, Kr, N_2, and He in addition to Ar.

Electrons are emitted from a directly heated spiral tungsten filament cathode, accelerated through a 1 cm diam hole of the grounded anode, which is biased positive with respect to the cathode, and collected by the grounded endplate target. Figure 2(a) shows the electron current at the endplate target (I_p) as a function of the filament heating power (P_f) for three different beam acceleration voltages (V_B). It can be seen from Fig. 2(a) that I_p is governed by temperature limited emission at lower P_f (where it monotonically increases as P_f is in-

TABLE I. Typical experimental parameters.

Gas used	Ar (He, N_2, Kr, Xe)
Pressure	$P=5\times10^{-6}\sim5\times10^{-5}$ Torr
Magnetic field	$B=40\sim280$ G
Endplate current	$I_p=10\sim1000$ μA
Beam voltage	$V_B<500$ V
For Ar 2×10^{-5} Torr, $I_p=100$ μA, $V_B=250$ V, $B=160$ G	
Beam density	$n_b\approx10^6$ cm^{-3}
Plasma electron density	$n_e\approx10^8$ cm^{-3}
Plasma ion density	$n_i\approx10^7$ cm^{-3}
Electron temperature	$T_e\approx4$ eV
Ion parallel temperature	$T_{i\parallel}>0.03$ eV
Ion perpendicular temperature	$T_{i\perp}\approx5$ eV
dc radial electric field	$E_{ro}\approx4.7$ V/cm
Plasma potential difference	$\Delta\Phi\approx5.0$ V
Measured instability frequency	$f_1=48.3$ kHz ($m=1$: measured)
Ion cyclotron frequency	$f_{ci}=6.1$ kHz
Ion plasma frequency	$f_{pi}=104$ kHz
Electron plasma frequency	$f_{pe}=89.8$ MHz
Electron $E\times B$ frequency	$f_{E\times B}=940$ kHz ($m=1$)
Electron diamagnetic frequency	$f^*=3.0$ MHz ($m=1$)
Azimuthal phase velocity	$\omega_1/k_\theta=1.3\times10^5$ cm/sec ($k_\theta=2$ cm^{-1})
Axial phase velocity	$\omega_1/k_z=8.3\times10^6$ cm/sec ($k_z\approx0.03$ cm^{-1})
Ion acoustic velocity	$c_s=3.1\times10^5$ cm/sec
Electron thermal velocity	$v_{the}=1.2\times10^8$ cm/sec
Collision frequency	
Electron–neutral elastic[9]	$\nu_{en}=6.6\times10^4$ sec^{-1}
Ion–neutral charge exchange[9,10]	$\nu_{in}=2.2\times10^2\sim2.9\times10^3$ sec^{-1}
Electron–ion[11]	$\nu_{ei}=2.5\times10^2$ sec^{-1}
Collision mean-free-path	
Electron–neutral elastic[9]	$\lambda_{en}=1.8\times10^3$ cm ($\sigma_{en}=8.4\times10^{-16}$ cm^2)
Ion–neutral charge exchange[9,10]	$\lambda_{in}=1.7\times10^2$ cm ($\sigma_{in}=9.0\times10^{-15}$ cm^2)
Electron–ion[11]	$\lambda_{ei}=5.4\times10^5$ cm
Electron Debye length	$\lambda_D=0.15$ cm
Larmor radius	
Electron	$r_{Le}=0.04$ cm
Ion	$r_{Li}=12.5$ cm ($T_{i\perp}=5$ eV)

creased) and governed by space-charge limited emission at higher values of P_f (where it shows saturation behavior). Experiments were performed at $V_B=250$ V and $I_p=10$ to 1000 μA. These parameters are in the temperature limited emission region.

Table I summarizes typical experimental parameters.

A. Density measurements

Beam and plasma densities are measured by the Langmuir probe. Since the typical gas pressures are low, the probe characteristics show clear distinctions (a pronounced knee) between the ion saturation current (I_{is}), the beam electron current (I_{beam}) and the electron saturation current (I_{es}). Figure 2(b) shows probe characteristics measured by a 2×2 mm square disc probe (0.05 mm in thickness). When the disc is normal to the electron beam,

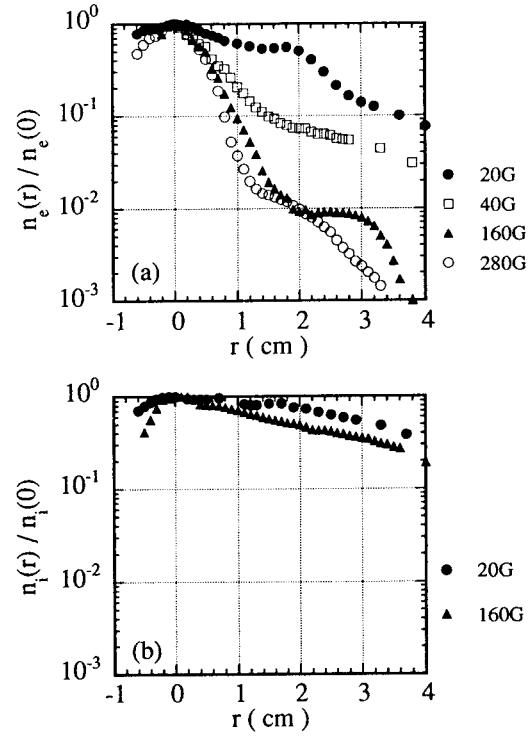

FIG. 3. The measured magnetic field dependence of the radial profiles of (a) n_e and (b) n_i. At $B=160$ G, n_e has a 1.0 cm (FWHM) Gaussian profiles, while n_i shows a broad profile from the beam center to the chamber wall ($r=5$ cm). The n_e profile becomes broader at the lower B, while that of n_i is nearly unchanged with B. $P=2\times10^{-5}$ Torr, $I_p=500$ μA.

we observe a clear beam component with the probe biased more negative with respect to $-V_B=-250$ V in this measurement. When the disc is parallel to the electron beam, a very small beam component collected by the edge area of (0.05 mm thickness×2 mm) the probe is observed.

In a magnetic field, the electron saturation current is reduced due to the reduced diffusion coefficient across the field.[12] Therefore, the absolute magnitude of the plasma electron density, n_e, is not reliable. However, as long as B is constant, the relative magnitude of n_e as a function of radius r or I_p, etc. are thought to be correct. On the other hand, the plasma ion density, n_i, is overestimated in our measurement due to the thick sheath effect.[12] Since we have to bias the probe more negatively, with respect to $-V_B=-250$ V to collect ions, we expect to have effective probe surface area being larger than the actual probe size because of the thick sheath. If we extrapolate the ion current at the plasma potential, we find nearly an order of magnitude lower current compared to the current measured at $V_{pr}=-280$ V. Here, V_{pr} is the probe bias voltage. Because of these uncertainties in both electron and ion density measurements by the probe, we choose not to determine the absolute plasma densities from probe measurements alone. On the other hand the absolute value of the difference between the electron and ion densities (n_e–n_i) can be obtained from the measurement of the plasma potential Φ. Since the relative radial profiles of the densities are thought to be correct, we adjust the peak density of the

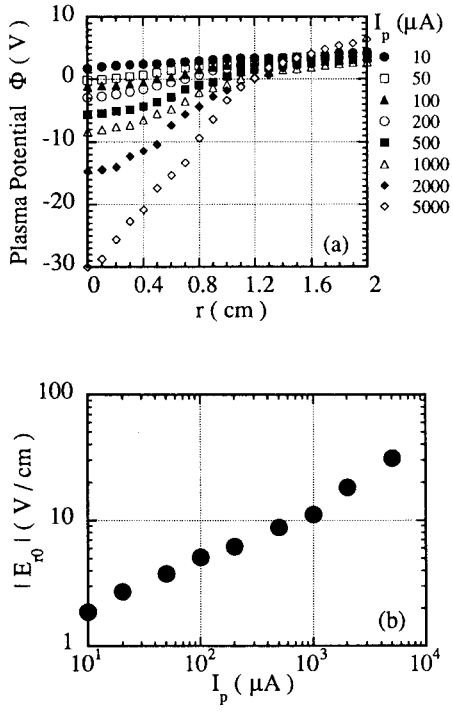

FIG. 4. (a) The radial profiles of Φ as a function of I_p measured by the emissive probe at $P=2\times10^{-5}$ Torr. (b) I_p dependence of the calculated maximum $|E_{r0}|$ ($r\approx0.5$ cm).

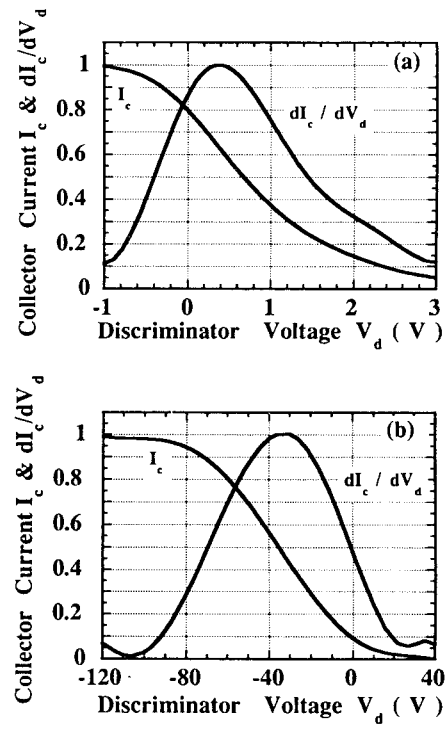

FIG. 5. The measured normalized collector current (I_c) and its derivative (dI_c/dV_d) versus discriminator voltage (V_d) for (a) $I_p=1$ μA and (b) $I_p=7000$ μA. $P=2\times10^{-5}$ Torr, $r=1.5$ cm.

electrons and ions to fit the measured potential profile. This fitting procedure indicates that the plasma is electron rich on axis and ion rich outside of the electron beam.

The measured magnetic field (B) dependence of the radial profiles of n_e and n_i are shown in Figs. 3(a) and 3(b), respectively. At $B=160$ G, n_e (and n_b, not shown in the figure) have 1 cm (FWHM), Gaussian profiles, while n_i shows a broad profile from the beam center to the chamber wall ($r=5$ cm). The electron profile, $n_e(r)$, becomes broader at lower values of B, whereas the ion density profile is nearly unchanged. This is because the ions are unmagnetized ($r_{Li} \gg r_p$, where r_{Li} is the ion Larmor radius and $r_p=0.5$ cm is the plasma size) even at $B=250$ G, while the electrons are weakly magnetized ($r_{Le} \leqslant r_p$, where r_{Le} is the electron Larmor radius) at the lower values of B but are strongly magnetized ($r_{Le} \ll r_p$) for high values of B.

B. Plasma potential measurement

The difference between the electron and ion radial density profiles implies the existence of a radial dc electric field, E_{r0}, which we deduced by measuring the radial profile of the plasma potential, Φ, with an emissive probe[12] (0.05 mm diam tungsten wire) heated by a dc power supply. The I–V trace of the emissive probe is taken to confirm that the emission current is much larger than the collection current, and the floating potential of the probe matches well with the plasma potential. The radial profiles of Φ as a function of I_p are shown in Fig. 4(a), and the calculated maximum $|E_{r0}|$ ($=|-\nabla\Phi|$) versus I_p is shown in Fig. 4(b). We find that $|E_{r0}|$ increases monotonically with I_p but decreases with P (not shown). The difference between the local electron and ion densities, n_e-n_i, calculated using Poisson's equation, is positive in the beam region and negative outside the beam. The shape of the electron and ion density profiles support this notion.

C. Temperature measurements

The ion perpendicular temperature, $T_{i\perp}$, is measured by an energy analyzer which consists of two mesh grids and a collector plate. It is 1.5 cm diam, 1.25 cm long and faces radially inward on a radially movable shaft. The first grid is left to float to repel most electrons and pass ions. The collector plate is biased to $V_c=-67.5$ V to collect ions and repel electrons. Figure 5 shows the measured normalized collector current (I_c) and its derivative (dI_c/dV_d) versus discriminator voltage (V_d) for $I_p=1$ μA [Fig. 5(a)] and $I_p=7000$ μA [Fig. 5(b)]. The perpendicular ion "temperature" $T_{i\perp}$ calculated from the e-folding bias voltage in the dI_c/dV_d curve is shown in Fig. 6(a) as a function of I_p. The dc plasma potential difference $\Delta\Phi$, between $r=2.0$ and 0 cm measured by the emissive probe, is also shown in this figure. A good agreement between $T_{i\perp}$ and $\Delta\Phi$ is suggestive of $T_{i\perp}$ as being the characteristic kinetic energy of the ions as they rattle back and forth in the radial potential well. The radial position dependence of $T_{i\perp}$ is shown in Fig. 6(b). The largest value of $T_{i\perp}$ is at the center of the chamber as expected. Although the parallel component of the ion temperature was not measured, we expect $T_{i\parallel} \ll T_{i\perp}$ because ion–ion and ion–electron equilibrium

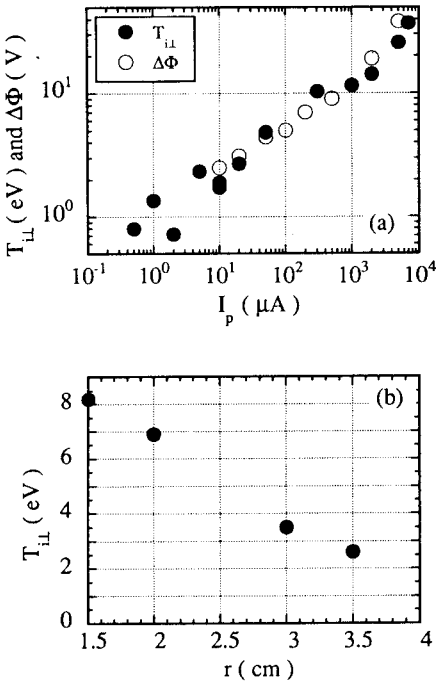

FIG. 6. T_{iL} measurements. (a) Dependence of T_{iL} on I_p (closed circle). T_{iL} is calculated from the e-folding bias voltage in the dI_e/dV_d curve measured at $r=1.5$ cm. The dc plasma potential difference, $\Delta\Phi$, between $r=2.0$ cm and $r=0$ cm measured by emissive probe is also shown (open circle). A good agreement between T_{iL} and $\Delta\Phi$ is obtained. (b) The radial position dependence of T_{iL}. T_{iL} is larger at the central region. $P=2\times10^{-5}$ Torr, $I_p=500$ μA.

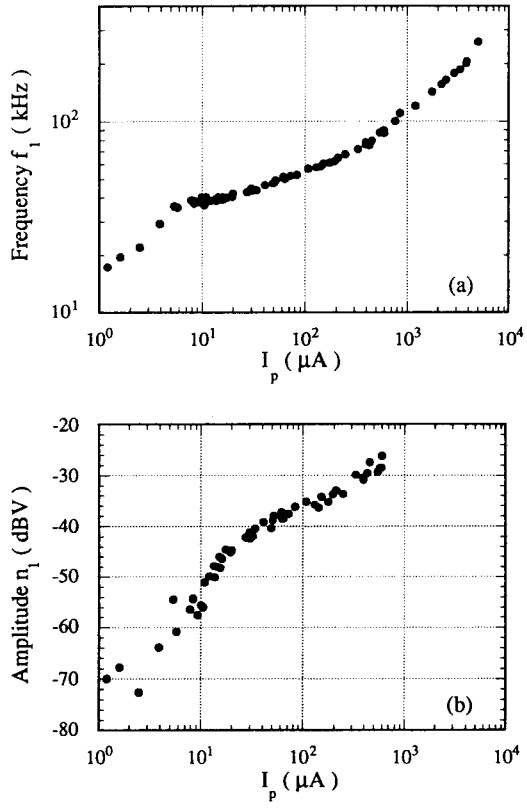

FIG. 7. A plot of the (a) M_1 mode frequency f_1 and (b) the spectral amplitude n_1 versus I_p. $P=2\times10^{-5}$ Torr, $r=0.5$ cm.

rate is much smaller than the ionization (or loss) rate. The plasma electron temperature measured by the Langmuir probe is $\simeq 4$ eV.

D. Instability measurements

By varying the gas pressure (P) or the endplate current (I_p), a low-frequency mode M_1 with a frequency f_1, between the ion cyclotron (f_{ci}) and the ion plasma (f_{pi}) frequencies ($f_{ci} \ll f_{pi}$) is excited. Most of the measurements reported below were made with unbiased, grounded cylindrical Langmuir probes (0.5 mm in diameter and ~ 2 mm in length). However, the same results, with much reduced amplitudes, can be obtained with probes biased to give the ion saturation current. The real time oscillating signals were recorded with a transient recorder (12 bits resolution and 2 MHz maximum sampling rate). The frequency spectra were obtained both by performing fast Fourier transforms (FFT) on the real-time signal and with an HP model 3561A spectrum analyzer terminated by a 1 kΩ resistor. We confirmed that there are no electron plasma or electron cyclotron oscillations excited in our experiment. When the gas pressure is increased above 10^{-4} Torr and I_p above 1000 μA, these relatively higher frequency oscillations can clearly be seen.

A plot of the frequency f_1 and the spectral amplitude n_1 of the M_1 mode as a function of the electron current collected by the endplate target I_p is shown in Fig. 7. The peak amplitude of this mode, as inferred by measuring the

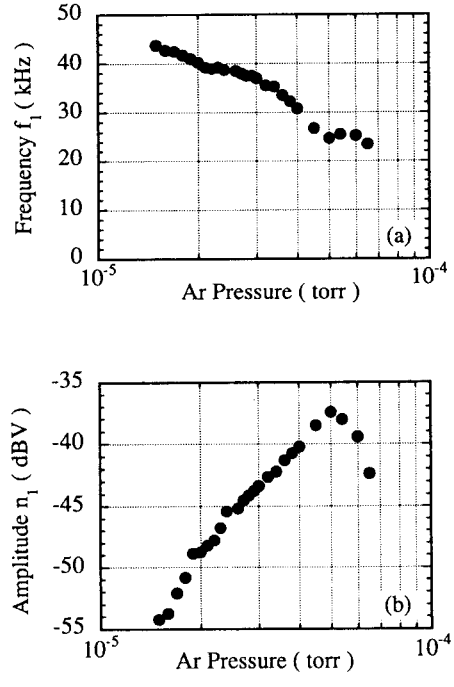

FIG. 8. The Ar pressure dependence of (a) f_1 and (b) n_1. $I_p=16$ μA, $r=0.5$ cm.

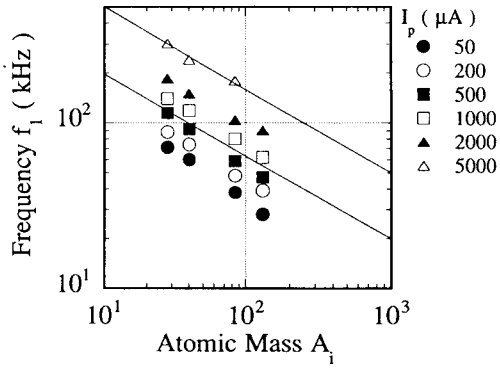

FIG. 9. Atomic mass dependence of the instability frequency for six different values of I_p in μA. It is clear that f_1 has a $1/\sqrt{M}$ dependence. $P=10^{-5}$ Torr, $r=0.3$ cm.

fluctuating value of the ion saturation current, can approach $\tilde{n}_i/n_0 \simeq 1$. This occurs for $I_p > 7000$ μA. However, for these values of I_p the plasma is already quite turbulent due to a cascade of sideband instabilities thought to be induced by trapped ions.[13] Furthermore, harmonics of f_1 are observed up to the seventh harmonic.[14] As will be seen later, the M_1 mode is a mode with an azimuthal mode number $m=1$. We speculate that the harmonics of f_1 represent distortion of the wave shape to include higher azimuthal mode numbers but this conjecture awaits further confirmation. Indeed at times the spectral power density of the second harmonic frequency ($m=2$ mode) can be somewhat greater than that of the fundamental M_1 mode.

Figure 8 shows that Ar pressure dependence of f_1 and n_1. In this measurement, I_p was kept constant at 16 μA. Whereas f_1 increases with increasing I_p, it is found to decrease as P is increased. Here it is worth recalling that E_{r0} increases with increasing I_p but shows a decrease as P is increased. The spectral amplitude of M_1 is, however, seen to increase with P until P exceeds 5×10^{-5} Torr. At this pressure, the frequency spectrum of M_1 becomes broader and the signal-to-noise ratio becomes smaller. Above 7×10^{-5} Torr, the plasma becomes quite turbulent[13] and one can no longer distinguish the frequency peaks of M_1 mode and its harmonics.

The ion mass (M) dependence of f_1 is shown in Fig. 9 for six different values of I_p. It is clear that f_1 has a $1/\sqrt{M}$ dependence.

Figure 10(a) shows the radial profile of the M_1 mode frequency, f_1. It was observed that f_1 is almost constant from the beam center to the chamber wall ($r=5$ cm) suggesting that the M_1 mode is a characteristic eigenmode of the system, not a local mode. Figure 10(b) shows that the M_1 mode has a spectral amplitude peak at the beam edge.

The azimuthal wave number of the M_1 mode, k_θ, was measured by three probes located 90° to one another at the same radial and axial position. From the phase difference between the three probes, we concluded that M_1 has an azimuthal mode number $m=1$ in the direction of the $E\times B$ drift or the electron diamagnetic drift. Thus $k_\theta=m/r$ is 2 cm^{-1}. The component k_z of M_1 (in the direction of the B field) was determined, by measuring the phase difference between a fixed probe and an axially movable probe, to be ~ 0.03 cm^{-1}.

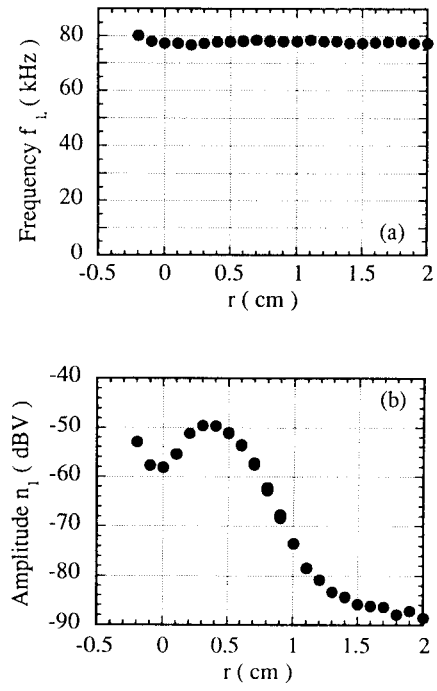

FIG. 10. The radial profiles of (a) f_1 and (b) n_1. Frequency f_1 is almost constant from the beam center to the chamber wall suggesting that the M_1 mode is a global mode. The n_1 peak is at the beam edge and the wave number measurements show that M_1 is an azimuthally propagating mode. $P=1\times10^{-5}$ Torr, $I_p=100$ μA.

E. Ion azimuthal velocity, $v_{\theta i}$, measurement

The ion azimuthal velocity, $v_{\theta i}$, is measured by one-sided-probe technique.[15] A probe is shielded on one side and biased to collect the ion saturation current. When the probe is faced away from the ion rotation direction, only the ion saturation current, I_{is}, is collected. When the probe is faced to the rotation direction, both I_{is} and the current caused by ion drift, $I_{i\theta}$, are collected. The difference in the currents ΔI is equal to $I_{i\theta}$ and related to $v_{\theta i}$ by $v_{\theta i}=\Delta I c_s/I_{is}$, where $c_s=\sqrt{T_e/M}$.

Figure 11 shows the measured f_1 and the ion rotation frequency $f_{\theta i}=v_{\theta i}k_\theta/2\pi$. Here we have taken $k_\theta=1/r$ and $r=0.5$ cm which is the radius at which the M_1 mode has a maximum spectral amplitude. The calculated value of $f_{\theta i}$ shows the same general trend as f_1 and agrees within a factor of two for I_p [Fig. 11(a)], P [Fig. 11(b)] and B [Fig. 11(c)] scans. Also shown in Fig. 11 is f_{Ei}, the calculated effective ion $E\times B$ drift frequency which will be discussed later in the paper. However, we now show, based on theoretical considerations, that the modified Simon–Hoh instability (MSHI) is a candidate for the instability observed in our experiment.

III. THEORETICAL CONSIDERATIONS

In this section, we describe theoretical considerations of the MSHI. In order to clarify (a) the plasma parameter regions of the MSHI and (b) the differences with other instabilities, we first derive a general expression for the electrostatic oscillations, which includes effects of B fields, dc electric fields, plasma temperature, density gradients, and collisions. Then, we apply our experimental conditions to the equation and show the dispersion relation of the MSHI. In the Appendix, we show that the dispersion relation of several well-known instabilities can be obtained from the equation by choosing proper limits.

A. General fluid theory

We assume Cartesian geometry with a uniform magnetic field $\mathbf{B}_0 = B_0\hat{z}$. We look for electrostatic oscillations of fluctuating potential ϕ and density perturbation $\tilde{n}$ given by

$$\phi = \phi(x)e^{i(k_y v_y + k_z v_z - \omega t)}, \tag{4}$$

$$\tilde{n} = \tilde{n}(x)e^{i(k_y v_y + k_z v_z - \omega t)}; \tag{5}$$

and the fluctuating electric field is given by

$$E_{1x} = -\frac{d\phi}{dx} = -\phi', \tag{6}$$

$$E_{1y} = -ik_y\phi. \tag{7}$$

The dc electric field and density are $\mathbf{E}_0 = E_0\hat{x}$ and $n_0 = n_0(x)$, respectively. We use the linearized equations of motion

$$n_{j0}m_j\left(\frac{\partial \mathbf{v}_{j1}}{\partial t} + (\mathbf{v}_{j0}\cdot\nabla)\mathbf{v}_{j1} + (\mathbf{v}_{j1}\cdot\nabla)\mathbf{v}_{j0}\right) + n_{j1}m_j(\mathbf{v}_{j0}\cdot\nabla)\mathbf{v}_{j0} = s_j e n_{j0}(\mathbf{E}_1 + \mathbf{v}_{j1}\times\mathbf{B}_0) + s_j e\tilde{n}_j(\mathbf{E}_0 + \mathbf{v}_{j0}\times\mathbf{B}_0) - T_j\nabla\tilde{n}_j - m_j n_{j0}\mathbf{v}_{j1}\nu_j, \tag{8}$$

and the continuity equation

$$\frac{\partial \tilde{n}_j}{\partial t} + (\mathbf{v}_{j0}\cdot\nabla)\tilde{n}_j + n_{j0}\nabla\cdot\mathbf{v}_{j1} + (\mathbf{v}_{j1}\cdot\nabla)n_{j0} = 0, \tag{9}$$

for plasma ions, plasma electrons, and beam electrons, together with the local approximation, $\phi'' = \phi' = 0$ and $\tilde{n}'' = \tilde{n}' = 0$, where $j = i$ (ion), e (plasma electron), and b (beam electron), $s_i = 1$, $s_e = s_b = -1$, ν_j is the collision frequency. The density gradient is $k_{nj} = |n'_{j0}/n_{j0}| = |(1/n_{j0})(dn_{j0}/dx)|$, where $n'_{j0} < 0$. Since collisions in the perpendicular equation give classical diffusion that is negligible, we consider collisions only in the $\hat{z}$ direction. We find

$$\frac{\tilde{n}_j}{n_{j0}} = \frac{s_j e\phi}{m_j}\left\{\left(\frac{k_y^2}{\bar{\omega}^2 - \Omega_j^2} + \frac{k_z^2}{\bar{\omega}^2 + i\nu_j\bar{\omega}} - \frac{s_j\Omega_j k_{nj}k_y/\bar{\omega}}{\bar{\omega}^2 - \Omega_j^2}\right) \Big/ \left[1 - \frac{T_j}{m_j}\left(\frac{k_y^2}{\bar{\omega}^2 - \Omega_j^2} + \frac{k_z^2}{\bar{\omega}^2 + i\nu_j\bar{\omega}} + \frac{k_{nj}^2 - s_j\Omega_j k_{nj}k_y/\bar{\omega}}{\bar{\omega}^2 - \Omega_j^2}\right)\right]\right\}, \tag{10}$$

where $\Omega_j = |s_j eB_0/m_j|$ is the cyclotron frequency and $\bar{\omega}_j = \omega - \mathbf{k}\cdot\mathbf{v}_{j0}$ is the frequency in the species' rest frame. The drift term $\mathbf{k}\cdot\mathbf{v}_{j0}$ is expressed as

$$\mathbf{k}\cdot\mathbf{v}_{b0} = k_z v_{\text{beam}} + k_y v_{E\times Be} + k_y v_{bd} = k_z v_{\text{beam}} + \omega_{Eb} + \omega_b^*, \tag{11}$$

$$\mathbf{k}\cdot\mathbf{v}_{e0} = k_y v_{E\times Be} + k_y v_{ed} = \omega_{Ee} + \omega_e^*, \tag{12}$$

$$\mathbf{k}\cdot\mathbf{v}_{i0} = k_y v_{E\times Bi} + k_y v_{id} = \omega_{Ei} + \omega_i^*, \tag{13}$$

where v_{beam} is the beam velocity, $\omega_{Ej} = k_y v_{E\times Bj}$ is the $E\times B$ drift frequency and $\omega_j^* = k_y v_{jd} = -s_j(T_j/eB_0)k_{nj}k_y$ is the diamagnetic drift frequency. For convenience we use ω_E and ω^* for the electron $E\times B$ and the electron diamagnetic drift frequency, respectively.

Now we identify y with θ and x with r in cylindrical geometry, and then apply our experimental conditions. In our experiment, the following plasma conditions are present: (a) Electrons are magnetized while the ions are essentially unmagnetized ($\Omega_i \ll \omega \ll c_e k_\theta \ll \Omega_e$, where $c_e = \sqrt{T_e/m}$); (b) ions and beam electrons are cold ($T_i, T_b \simeq 0$) while the plasma electrons are not cold ($T_e \neq 0$); (c) the collisions with neutral atoms are negligible ($\nu_{en}, \nu_{in} \simeq 0$); and (d) $k_{ne} = k_{nb} \gg k_\theta \gg k_z, k_{ni}$. It can be seen that the beam electrons follow Eq. (A2) with the third term on the right-hand side being dominant because of small k_z and large Ω_e; the plasma electrons are expressed by the modified Boltzmann relation for the $k_z \simeq 0$ case, Eq. (A7); and the plasma ions are reduced to Eq. (A10) with nonzero azimuthal drift, which will be described later. These relations are given as

$$\frac{\tilde{n}_b}{n_{b0}} = \frac{e\phi}{m}\frac{k_{nb}k_\theta}{\bar{\omega}_b\Omega_e} = \frac{e\phi}{T_e}\frac{\omega^*}{\omega - \omega_E - k_z v_{\text{beam}}}, \tag{14}$$

$$\frac{\tilde{n}_e}{n_{e0}} = \frac{e\phi}{T_e}\frac{\omega^*}{\omega - \omega_E}, \tag{15}$$

$$\frac{\tilde{n}_i}{n_{i0}} = \frac{e\phi}{T_e}\frac{c_s^2 k_\theta^2}{(\omega - \omega_{\theta i})^2}, \tag{16}$$

where $\omega_b^* = \omega^*$, $\omega_{Eb} = \omega_E$, $\omega^* = v_{ed}k_\theta$, $\omega_E = v_{E\times Be}k_\theta$ and $\omega_{\theta i} = v_{\theta i}k_\theta$, which is the mean azimuthal ion drift frequency.

1. Plasma approximation

For quasineutral perturbations, we take $\tilde{n}_e + \tilde{n}_b = \tilde{n}_i$, and we obtain

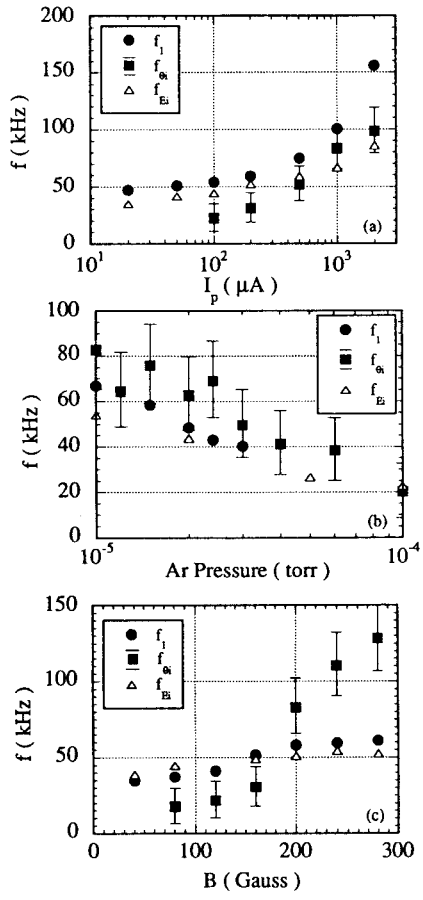

FIG. 11. The dependence of various frequencies on experimental parameters. (a) I_p, (b) P, and (c) B dependence of f_1, $f_{\theta i}$, and f_{Ei}. Here, $f_{\theta i}$ is the measured ion rotation frequency by the one-sided probe and expressed as $f_{\theta i}=v_{\theta i}k_\theta/2\pi$, where $k_\theta=1/r_1=2\ \mathrm{cm}^{-1}$ and $r_1=0.5$ cm is the radius at which M_1 amplitude is maximum. And f_{Ei} is the effective ion $E\times B$ drift frequency calculated from Eq. (52).

$$\frac{1}{k_\theta^2\lambda_D^2}\left((1-a)\frac{\omega^*}{\omega-\omega_E}+a\frac{\omega^*}{\omega-\omega_E-k_z v_{\mathrm{beam}}}\right)=\frac{\omega_{pi}^2}{(\omega-\omega_{\theta i})^2}, \tag{17}$$

where $\lambda_D=\sqrt{T_e/4\pi n_{e0}e^2}$ is the electron Debye length and $a=n_{b0}/n_{i0}$. When $a\ll 1$, neglecting the beam term,[16] we obtain

$$\frac{1}{k_\theta^2\lambda_D^2}\frac{\omega^*}{\omega-\omega_E}=\frac{\omega_{pi}^2}{(\omega-\omega_{\theta i})^2}. \tag{18}$$

Equation (18) is solved to give

$$\omega_R=k_\theta v_{\theta i}+\frac{c_s^2k_\theta^2}{2\omega^*}\simeq k_\theta v_{\theta i}, \tag{19}$$

$$\omega_I=\sqrt{c_s^2k_\theta^2\frac{(\omega_E-\omega_{\theta i})}{\omega^*}-\frac{c_s^4k_\theta^4}{4\omega^{*2}}}\simeq\sqrt{\frac{c_s^2k_\theta^2(\omega_E-\omega_{\theta i})}{\omega^*}}, \tag{20}$$

where ω_R and ω_I are the real and the imaginary parts of the instability frequency, respectively. This shows that when $v_{\theta i}<E_{r0}/B_0$, and $\omega_E/\omega^*>0$ we can have an excitation of a fluid instability. Note that the perpendicular phase velocity is nearly $v_{\theta i}$ with a small correction due to the second term in Eq. (19).

2. Poisson's equation

Now we apply Eqs. (15) and (16) to Poisson's equation

$$-\nabla^2\phi=4\pi e(\tilde{n}_i-\tilde{n}_e), \tag{21}$$

where we have neglected the beam components. We find

$$1=\frac{\omega_{pi}^2}{(\omega-\omega_{\theta i})^2}-\frac{1}{k_\theta^2\lambda_D^2}\frac{\omega^*}{\omega-\omega_E}, \tag{22}$$

where we have neglected Ω_i relative to ω. The roots for this dispersion relation are expressed by the Buneman instability type solution; i.e., the growth of the instability occurs as a result of the interaction between the fast (positive energy) wave on the ions and the slow (negative energy) wave on the electrons.[11] In the case of the MSHI, fast and slow ion waves given by

$$\omega=k_\theta v_{\theta i}\pm\omega_{pi} \tag{23}$$

and a slow electron wave given by

$$\omega=k_\theta v_E-\frac{\omega^*}{k_\theta^2\lambda_D^2} \tag{24}$$

interact together. Figure 12 shows the real part $\omega_R'=\omega_R/\Omega_i$ [Fig. 12(a)] and the imaginary part $\omega_I'=\omega_I/\Omega_i$ [Fig. 12(b)] of the instability frequencies of Eq. (22) as a function of $k'=k_\theta v_E/\Omega_i$. Since k_θ is fixed to the $m=1$ mode, we consider that changes in k' are due to changes in v_E and treat $\omega^*/k_\theta^2\lambda_D^2$ as unchanged from case to case. When $k'\leqslant 0$ or $k'\geqslant 1250$, there are three real frequency roots that indicate the plasma is stable. While at $0\leqslant k'\leqslant 1250$, we find only one real frequency root and two complex frequency roots, which correspond to a growing wave ($\omega_I>0$) and a decaying wave ($\omega_I<0$). In our experiment, $k'=155$ (see Table I) and there exists an unstable root. Note that at $k'<1100$, ω_R of the unstable root is expressed exactly as $\omega_R=k_\theta v_{\theta i}$, which is the same as the plasma approximation result. Deviation from the $\omega_R=k_\theta v_{\theta i}$ occurs when $\omega^*/k_\theta^2\lambda_D^2\leqslant k_\theta v_E$, or $k_\theta^2\lambda_D^2>1$. This is the same condition as the case when the plasma approximation is not valid. In our experimental conditions, since $\omega^*/k_\theta^2\lambda_D^2>k_\theta v_E$ is always satisfied, the plasma approximation gives correct results. Note that in the case $k_\theta v_{\theta i}=0$, the maximum growth of the unstable root occurs when $\omega\simeq k_\theta v_E\simeq\omega_{pi}$. This root corresponds to the flute-like drift instability.[1,3,5]

B. Kinetic considerations

Now we consider kinetic effects on ions. Note that in the actual experiment, ions have large perpendicular excursions in the electrostatic well created by the magnetized radially localized electrons. The ion density response must therefore be obtained from an appropriate Vlasov equation. The unperturbed ion distribution, f_{i0}, is a function of the constants of motion, i.e., the perpendicular and parallel

energies $W_\perp=(M/2)(\dot{r}^2+r^2\dot{\theta}^2)+e\Phi(r)$, $W_\parallel=(M/2)\dot{z}^2$ and the θ-canonical momentum $P_\theta=Mr^2(\dot{\theta}+\Omega_i/2)$, where $\Omega_i=eB_0/M$ is the ion cyclotron frequency. Since the ion density is nearly uniform in space, f_{i0} may be chosen as a function of $W_\perp$ and $W_\parallel$ only. The perturbed Vlasov equation may now be solved in principle by following the characteristics:

$$\tilde{f}_i=-\int_{-\infty}^{t}\frac{e}{M}\mathbf{E}_1[\mathbf{r}'(t'),t']\cdot\frac{\partial f_{i0}}{\partial \mathbf{v}'}\,dt' \tag{25}$$

and the density perturbation obtained by the equation $\tilde{n}_i=\int \tilde{f}_i d^3v$. The exact eigenmode problem is quite complex because of the complicated zeroth-order ion orbits [determined by $\Phi(r)$ and B_0] and the radially nonlocal response of ions, which leads to integrodifferential operators. Considerable insight into the new physical effects introduced by large orbit excursions may, however, be obtained from an approximate kinetic theory that uses harmonic orbit approximations (exact for a parabolic potential well) and an appropriately averaged local radial response for the ions.

The unperturbed trajectory of ions is determined from a solution of the equations

$$\frac{d\mathbf{r}}{dt}=\mathbf{v}, \tag{26}$$

$$\frac{d\mathbf{v}}{dt}=\Omega_i(\mathbf{v}\times\hat{z})+\frac{eE_0}{M}\hat{r}. \tag{27}$$

When B_0 is large and ions are magnetized, the second term in the right-hand side of Eq. (27) represents the $E\times B$ drift term. On the other hand, when B_0 is small and ion orbits are mainly decided by the E_0 term, and by assuming a parabolic potential well

$$\Phi=-\Phi_0\left(1-\frac{r^2}{r_0^2}\right), \tag{28}$$

where $\Phi_0>0$, Eq. (27) is reduced to

$$\frac{d\mathbf{v}}{dt}=\Omega_i(\mathbf{v}\times\hat{z})-\Omega_R^2\mathbf{r}, \tag{29}$$

where $\Omega_R=\sqrt{2e\Phi_0/Mr_0^2}$ is the ion rattle frequency in the parabolic electrostatic well created by the electrons. In the case when $\Omega_R\gg\Omega_i$ is satisfied, ions are trapped in Φ and "magnetized" due to rattling in this potential well. In this situation, Ω_R takes the role of the cyclotron frequency, Ω_i, and $\Omega_i r\hat{\theta}$ the role of the $E\times B$ drift.[17]

Now we show the dispersion relations with the ion cyclotron oscillation and the $E\times B$ drift. Solving Eq. (25) for $T_{i\perp}\neq T_{i\parallel}$ ($T_{i\perp}\gg T_{i\parallel}$ simulates the rattle effect), the ion suspectibility χ_i is given by[18]

$$\chi_i=\frac{1}{k^2\lambda_{\mathrm{D}i}^2}\left[1+\sum_n\left(1+\frac{T_{i\parallel}}{T_{i\perp}}\frac{n\Omega_i}{\bar{\omega}-n\Omega_i}\right)\times[W(z_n)-1]I_n(b)e^{-b}\right], \tag{30}$$

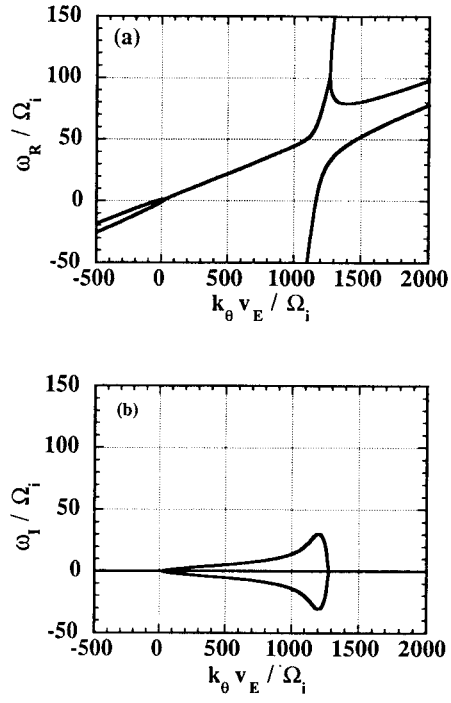

FIG. 12. Dispersion relation of the MSHI. (a) The real part and (b) the imaginary part of the instability frequencies.

where $z_n=(\bar{\omega}-n\Omega_i)/(k_z\sqrt{T_{i\parallel}/M})$, $\lambda_{\mathrm{D}i}=\sqrt{T_{i\parallel}/4\pi n_{i0}e^2}$, $b=k_\theta^2a^2$, $a=(1/\Omega_i)\sqrt{T_{i\perp}/M}$ is the finite Larmor radius (FLR) term, W is the plasma dispersion function, and $\bar{\omega}=\omega-k_\theta\langle v_{\theta i}\rangle$, where $\langle v_{\theta i}\rangle$ is the average ion $E\times B$ drift. The kinetic effects are negligible under our experimental conditions because when $k_z\approx 0$, $z_n\gg 1$, and $b\gg 1$ are satisfied, Eq. (30) is reduced to the unmagnetized limit

$$\chi_i=-\frac{\omega_{pi}^2}{\bar{\omega}^2}. \tag{31}$$

Using the plasma approximation $\chi_e=-\chi_i$, where the electron suspectibility, χ_e, is given by the fluid calculation, we obtain the dispersion relation

$$\frac{1}{k_\theta^2\lambda_{\mathrm{D}}^2}\frac{\omega^*}{\omega-\omega_E}=\frac{\omega_{pi}^2}{\bar{\omega}^2}. \tag{32}$$

Equation (32) is identical to the fluid calculation result, as shown in Eq. (18).

C. Comparison with other instabilities

1. Modified two-stream instability (MTSI) and flutelike drift instability (FDI)

A dispersion relation for the intermediate frequency ($f_{ci}\ll f\ll f_{ce}$) electrostatic instabilities driven by relative electron–ion drift across an external axial magnetic field[1–5] is expressed as

$$1+\chi_e+\chi_i=0, \tag{33}$$

$$\chi_e=\frac{\omega_{pe}^2}{\Omega_e^2}\frac{k_\perp^2}{k^2}-\frac{\omega_{pe}^2}{(\omega-kv_{0e})^2}\frac{k_z^2}{k^2}+\frac{\omega_{pe}^2}{\Omega_e(\omega-kv_{0e})}\frac{k_n k_\perp}{k^2}, \tag{34}$$

$$\chi_i=-\frac{\omega_{pi}^2}{(\omega-kv_{0i})^2}, \tag{35}$$

where $k_n=|n_0'/n_0|$. When the density gradient term (the third term) is dominant over the k_z term (the second term) in χ_e, a dispersion relation for the flutelike drift instability (FDI)[1,3,5] is derived. Equation (33) is reduced to the modified two-stream instability (MTSI)[2-4] when the condition is reversed. The instability that we have observed is $k_z\approx 0$, $k_n\neq 0$ mode. Therefore, it is similar to the FDI. For the experimental condition of $\omega_{pe}^2\ll\Omega_e^2$, $k_z=0$, Eq. (34) is reduced to

$$\chi_e=\frac{\omega_{pe}^2(k_n/k)}{\Omega_e(\omega-kv_{0e})}=\frac{1}{k^2\lambda_D^2}\frac{\omega^*}{\omega-kv_{0e}}, \tag{36}$$

which is the modified Boltzmann relation for $k_z=0$. The dispersion relation Eq. (33) is reduced to[19]

$$(\omega-kv_{0e})[(\omega-kv_{0i})^2-\omega_{pi}^2]=-\frac{1}{k^2\lambda_D^2}\omega^*(\omega-kv_{0i})^2. \tag{37}$$

When (1) $kv_{0e}\approx\omega_{pi}$, $\omega\approx\omega_{pi}$, and $kv_{0i}=0$, are satisfied, the FDI has its maximum growth rate. The maximum growth rate $\gamma_{\max}$ is calculated from Eq. (37) by assuming $\omega=\omega_{pi}+i\gamma$ $(\gamma/\omega_{pi}\ll 1)$:[19]

$$\gamma_{\max}^2=\frac{\omega^*\omega_{pi}}{2k^2\lambda_D^2}. \tag{38}$$

The FDI is understood as an instability caused by a coupling between an electron $E\times B$ drift wave in a nonuniform plasma and an ion plasma oscillation. No instabilities are found for the conditions (2) $\omega\approx kv_{0e}$, $\omega\ll\omega_{pi}$, and $kv_{0i}=0$, (3) $\omega\ll kv_{0e}$, $\omega\approx\omega_{pi}$, and $kv_{0i}=0$. The modified Simon–Hoh instability (MSHI) is a new unstable flute mode for (4) $\omega\approx kv_{0i}\ll\omega_{pi}$, kv_{0e}. A growth rate of the MSHI is calculated from Eq. (37) by assuming $\omega=kv_{0i}+i\gamma$ $(\gamma/kv_{0i}\ll 1)$,

$$\gamma^2=\frac{k^2c_s^2(kv_{0e}-kv_{0i})}{\omega^*}. \tag{39}$$

This growth rate is exactly the same as the ω_I shown in Eq. (20) when $k=k_\theta$, $\omega_E=k_\theta v_{0e}$ and $\omega_{\theta i}=k_\theta v_{0i}$. Many authors[1-5] considered only a relative electron–ion drift v_0 in their theory. However, none of them considered v_{0i} and v_{0e} separately, which is necessary to get the proper ω_R of the MSHI. Unlike the FDI, the MSHI is unstable even when the plasma approximation $(k^2\lambda_D^2\ll 1)$ is satisfied, and both the real and the imaginary parts of ω are independent of plasma density.

2. Antidrift mode

The antidrift instability (ADI)[20] is an intermediate frequency electrostatic instability in a weakly ionized inhomogeneous plasma with cold $(T_i=0)$ unmagnetized ions. Here we consider three cases as follows.

(a) When $k_z=0$ and $E_{r0}=0$, we obtain

$$\frac{\tilde{n}_e}{n_{e0}}=\frac{e\phi}{T_e}\frac{\omega^*}{\omega}, \tag{40}$$

$$\frac{\tilde{n}_i}{n_{i0}}=\frac{e\phi}{T_e}\frac{k_\perp^2c_s^2}{\omega^2}. \tag{41}$$

Equations (40) and (41), together with the plasma approximation, give a stable mode with a frequency $\omega_R=c_s^2k_\perp^2/\omega^*$, which is identical to Eq. (18) in Ref. 20. Note that this ω_R is the same as the second term of the real frequency of the MSHI, Eq. (19) (different by a factor of 2).

There are two possible instability mechanisms to make the antidrift mode unstable. One is collisions between electrons and the neutral gas, and the other is relative slippage between electrons and ions caused by the dc electric field.

(b) When $k_z\neq 0$, $E_{r0}=0$, and electron–neutral collisions are important, we get

$$\frac{\tilde{n}_e}{n_{e0}}=\frac{e\phi}{T_e}\frac{\omega^*+ik_z^2c_e^2/\nu_{en}}{\omega+ik_z^2c_e^2/\nu_{en}}, \tag{42}$$

and $\tilde{n}_i/n_{i0}$ is the same as Eq. (41). Equations (41) and (42), together with the plasma approximation, give an ADI, which Fridman predicted in his paper.[21]

(c) When $E_{r0}\neq 0$, $k_z=0$, $k_\perp=k_\theta$, and the ion azimuthal drift is neglected, we also get an unstable solution which is the same as the MSHI case with $k_\theta v_{\theta i}=0$, i.e.,

$$\omega_R=c_s^2k_\theta^2/2\omega^*, \tag{43}$$

$$\omega_I=\sqrt{\frac{c_s^2k_\theta^2\omega_E}{\omega^*}-\frac{c_s^4k_\theta^4}{\omega^{*2}}}\approx\sqrt{\frac{c_s^2k_\theta^2\omega_E}{\omega^*}}. \tag{44}$$

In the case of the MSHI, since $k_\theta v_{\theta i}\gg c_s^2k_\theta^2/2\omega^*$ is satisfied, the instability frequency ω_R shows a completely different dependence on the plasma parameters compared to the ADI, even though ω_I is the same. Therefore, the MSHI is classified as the ADI with E_{r0} and $v_{Ee}\gg v_{\theta i}\neq 0$.

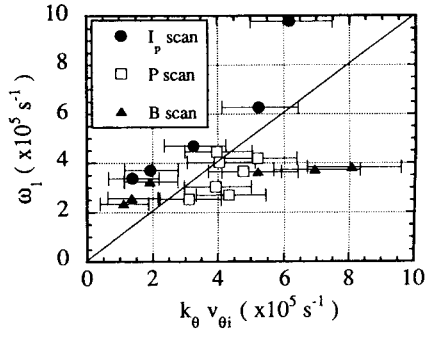

FIG. 13. The measured instability frequency ω_I versus the measured $k_\theta v_{\theta i}$ for I_p, P, and B scans, replotted from Fig. 11.

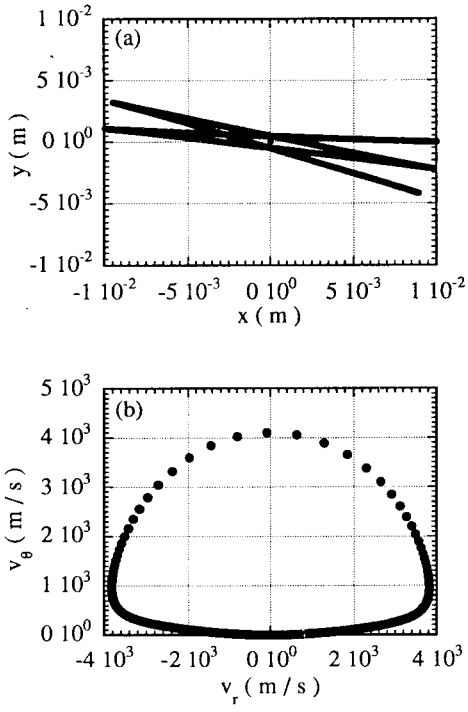

FIG. 14. Results of the ion orbit calculations. (a) A calculated ion orbit and (b) v_θ vs v_r for the measured dc plasma potential for $I_p=100\,\mu$A. The ion is assumed to be initially at rest ($v_r=v_\theta=0$) at $r=1$ cm.

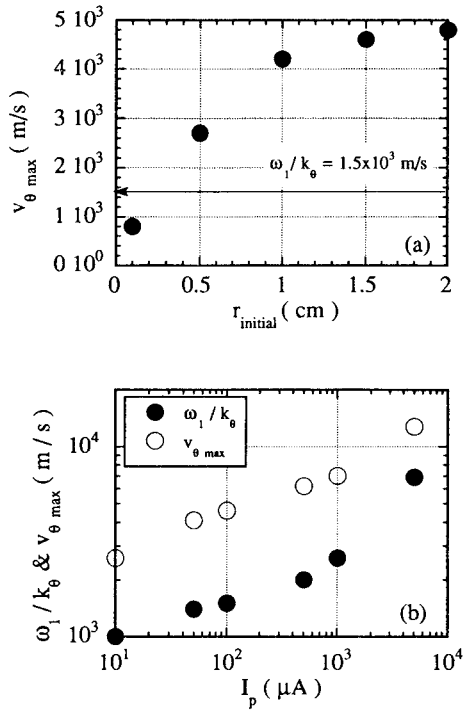

FIG. 15. Calculated maximum azimuthal ion drift velocity, $v_{\theta\max}$. (a) An initial position dependence of $v_{\theta\max}$ for the same potential profile as the Fig. 13 case. Note that $v_{\theta\max}$ saturates at $r>2$ cm, which is only a factor of 3 larger than ω_1/k_θ. The averaged fluid velocity of ions, $\langle v_{\theta i}\rangle$ seems to show a good agreement with ω_1/k_θ. (b) Variation of $v_{\theta\max}$ for the measured Φ profile at each I_p and the measured ω_1/k_θ. The initial position of ions is fixed at $r=1.5$ cm in the orbit calculation.

IV. DISCUSSION

As shown in Sec. III, the MSHI is unstable when $v_E > v_{\theta i}$ and the real part of the instability frequency is $\omega_R \simeq k_\theta v_{\theta i}$. Figure 13 shows the measured instability frequency ω_1 versus the measured $k_\theta v_{\theta i}$ for I_p, P, and B scans, replotted from Fig. 11. As mentioned in Sec. II E, ω_1 agrees with $k_\theta v_{\theta i}$ within a factor of 2. Therefore, experimentally we find, from the measurement of Φ, that v_E is a factor of 20 larger than ω_1/k_θ, whereas direct measurement of $v_{\theta i}$ shows that $v_{\theta i}\simeq\omega_1/k_\theta$; i.e., $v_E \gg v_{\theta i}$ and $\omega_1\simeq\omega_R$. We now carry out a simple ion orbit calculation, using the measured plasma potential profile [Fig. 4(a)], in order to explain how the ion azimuthal drift velocity $v_{\theta i}\simeq v_E/20$ is obtained.

A. Orbit calculation

Figure 14(a) shows an ion orbit in the measured potential well at $I_p=100\,\mu$A. We assume as a boundary condition that the ion is initially at rest at $r=1$ cm. The ion starts to move radially inward due to the E_{r0} field. As it approaches the center, it is pushed slightly radially outward due to the $v_\theta \times B_0$ force. After passing the center, the ion is decelerated and stops at the same radial position as the initial position.

Figure 14(b) shows v_θ vs v_r. At $t=0$, $v_r=v_\theta=0$ and the ion starts to gain negative v_r, and begins to rotate clockwise. The ion velocity v is governed by the law of conservation of energy, i.e.,

$$\frac{Mv_\theta^2}{2}+\frac{Mv_r^2}{2}=e\Delta\Phi, \tag{45}$$

where $\Delta\Phi$ is the dc plasma potential difference. For most of the time, v_r is much larger than v_θ because of the nearly straight line orbit of these ions. However, when an ion comes closest to the center, v_r approaches 0 and v_θ approaches $v_{\theta\max}$. At this point, Eq. (45) is reduced to

$$\frac{Mv_{\theta\max}^2}{2}=e\Delta\Phi. \tag{46}$$

It is this v_θ that decides the phase velocity of the azimuthally propagating mode M_1.

The dependence of $v_{\theta\max}$ on the initial radial position is shown in Fig. 15(a). We find that $v_{\theta\max}$ saturates at $r=2$ cm which is only a factor of 3 larger than ω_1/k_θ. In fact, the average fluid velocity of the ions $\langle v_{\theta i}\rangle$ seems to show a good agreement with ω_1/k_θ. Figure 15(b) shows a variation of $v_{\theta\max}$, assuming that the ions start at $r=1.5$ cm, using the measured Φ profiles, as shown in Fig. 4(a). The measured instability phase velocity, ω_1/k_θ, is also shown in Fig. 15(b). The calculated value of $v_{\theta\max}$ and ω_1/k_θ show a similar dependence on I_p over a wide range of values, and the two differ by about a factor of 3.

Now we explain the $M^{-0.5}$ ion mass dependence of the observed instability. As the ion motion is more or less

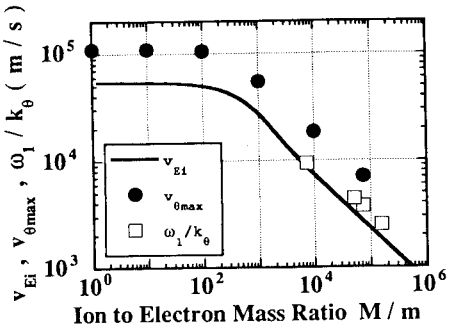

FIG. 16. Ion to electron mass ratio M/m dependence of the effective ion $E\times B$ drift velocity v_{Ei} calculated from Eq. (49) (solid line), $v_{\theta max}$ obtained from the ion orbit calculation (solid circle), and the measured instability phase velocity $v_1=\omega_1/k_\theta$ (open square).

governed by the dc potential profile, the instability frequency is expected to have a mass dependence

$$\omega_1 \simeq k_\theta \langle v_{\theta i} \rangle \propto \sqrt{\frac{2e\Delta\Phi}{M}} \propto M^{-0.5}. \tag{47}$$

B. Finite Larmor radius correction to the ion $E\times B$ drift

The solid circle in Fig. 16 shows the ion to electron mass ratio (M/m) dependence of $v_{\theta max}$, obtained from the simple ion orbit calculation shown in the previous section. In the figure, measured instability phase velocities, $v_1=\omega_1/k_\theta$, are also shown (the open square). These quantities, $v_{\theta max}$ and v_1, agree within a factor of 3. At $M/m < 300$, $v_{\theta max}$ has very weak mass dependence and corresponds to the $E\times B$ velocity. At $M/m > 300$, $v_{\theta max}$ shows a $1/\sqrt{M}$ dependence and corresponds to the potential domain velocity expressed by Eq. (46). We show a simple model to explain this smooth transition of $v_{\theta max}$ from the $E\times B$ velocity to the potential domain velocity.

Under a plane electric field, $E_0 \propto e^{-ik_\perp x}$, an averaged or effective electric field ($E_{\rm eff}$) over the ion gyrocycle and the Maxwellian distribution in $v_\perp$ is expressed as[22,23]

$$E_{\rm eff}=E_0 e^{-b} I_0(b), \tag{48}$$

where I_0 is the modified Bessel function of the first kind and $b = k_\perp^2 r_{Li}^2/2 = k_\perp^2 T_{i\perp} M/(eB_0)^2$. Mikhailovskii showed that Eq. (48) is valid not only for $b \ll 1$ but also for $b \gg 1$.[23] The averaged ion $E\times B$ drift velocity is, therefore, expressed as

$$v_{Ei}=\frac{E_0}{B_0} e^{-b} I_0(b). \tag{49}$$

Now we want to show that Eq. (49) gives a rough approximation for the phase velocity of MSHI or $v_{\theta i}$ in our cylindrical plasma. We consider a radial dc electric field E_{r0}. Radial profiles of E_{r0}, which are calculated from the measured Φ profiles, show zero at $r=0$ cm, maximum negative value at $r\approx 0.5$ cm, and zero again at $r\approx 2$ cm. We approximate the dc radial electric field with a sinusoidal field and compare the dc electric field scale length with an ion Larmor radius. We replace x with r and $k_\perp$ with $1/r_0$, where r_0 is a typical scale length of E_{r0}, and take $r_0=1.0$ cm.

When $b=r_{Li}^2/2r_0^2 \ll 1$, v_{Ei} is approximated by[22,23]

$$v_{Ei} \approx \frac{E_{r0}(1-b)}{B_0}. \tag{50}$$

This is the $E\times B$ velocity with a small finite Larmor radius (FLR) correction term. This means that the ions stay in a local radius and feel a local electric field.

When $b > 1$, v_{Ei} is expressed as[23]

$$v_{Ei} \approx \frac{E_{r0}}{B_0\sqrt{2\pi b}} = \frac{r_0 e E_{r0}}{\sqrt{2\pi T_{i\perp} M}}. \tag{51}$$

We approximate E_{r0} and $T_{i\perp}$ as $|E_{r0}| = |-\nabla\Phi| = k\Phi \approx \Delta\Phi/r_0$ and $T_{i\perp} \approx e\Delta\Phi$. Finally, for $b>1$ case, we obtain

$$v_{Ei} \approx \frac{1}{2\sqrt{\pi}} \sqrt{\frac{2e\Delta\Phi}{M}}. \tag{52}$$

In this case, ions do not complete their gyrocycle in one rattle motion. As shown in the previous section, an ion orbit shows a small deviation from a straight line, and this curvature corresponds to a part of a gyrocycle. Therefore, they can complete their gyrocycle with several rattle motions. This is equivalent to ions' traversing many wavelengths of the sinusoidal electric field in one gyrocycle. Equation (52) has the same dependence on Φ and M as the potential domain velocity shown in Eq. (46), i.e., the ion velocity obtained from the dc plasma potential.

Equation (49) is shown in Fig. 16 by the solid line as a function of M/m. We see that v_{Ei} shows a similar dependence on M/m as $v_{\theta max}$; i.e., v_{Ei} corresponds to the $E\times B$ velocity with a small FLR correction term [Eq. (50)] at $M/m < 300$, and corresponds to the potential domain velocity given by Eq. (52) at $M/m > 300$.

The effective ion $E\times B$ drift frequency $f_{Ei}=v_{Ei}k_\theta/2\pi$ calculated from Eq. (52) is shown in Fig. 11. We see that f_{Ei} agrees particularly well with the measured instability frequency (f_1) for the B scan and with the ion azimuthal drift frequency ($f_{\theta i}$) for the I_p scan. Furthermore, f_1 shows the same overall trend with I_p, P, and B as f_1 and $f_{\theta i}$. Therefore, we conclude that the phase velocity of the M_1 mode is expressed as v_{Ei}, the effective ion $E\times B$ drift velocity for large Larmor radius.

V. CONCLUSIONS

In conclusion, an intermediate frequency ($f_{ci} < f < f_{ce}$) electrostatic instability has been observed in an electron-beam produced plasma. We have identified the instability as a new instability, the modified Simon–Hoh instability, which has an instability mechanism similar to the Simon–Hoh instability. The instability occurs when the radial dc electric field and the density gradient are in the same direction. The instability phase velocity is decided by the ion azimuthal drift velocity, which is explained as the ion $E\times B$ drift velocity with the finite ion Larmor radius correction. We have investigated this new instability through theory and experiments.

The experimental findings can be summarized as follows.

(1) The measured ion azimuthal velocity, $v_{\theta i}$, is in reasonable agreement with the phase velocity of the M_1 mode, $v_1=\omega_1/k_\theta$, as expected for the MSHI.

(2) By using the measured plasma potential profile, it is found that the calculated $v_{\theta\max}$ shows good agreement with v_1. In this calculation, it is assumed that the ions are at rest at the initial position. In the experiments, the ion orbit is approximated by a straight line with a very small deviation due to $v\times B$ force.

(3) The dependence of f_1 on ion mass and the ion perpendicular temperature $T_{i\perp}$ are measured. It can be shown that they are simply expressed by $e\Delta\Phi\approx T_{i\perp}\approx Mv_i^2/2$. These results are expected from the orbit calculation.

(4) We have shown that the calculated $v_{\theta i}$ can simply be approximated by the ion $E\times B$ velocity v_{Ei}, expressed by Eq. (49), for a wide range of ion mass ratios M/m by assuming $T_{i\perp}\approx e\Delta\Phi$. The measured v_1 also agrees well with Eq. (49). The electron $E\times B$ drift velocity is simply given by $v_{Ee}=E_{r0}/B$, because of the small electron Larmor radius. A difference of 20 between the electron $E\times B$ and the ion azimuthal velocity is easily explained by Eq. (49).

Finally, we point out that in this paper we have discussed only the steady state nature of the MSHI. We have carried out experiments to illustrate the transient behavior (growth) of this instability. Clearly one of the crucial questions that has to be answered is how are the steady state ion and electron density profiles established. In other words, what is the ion heating mechanism that leads to ions spreading out in the radial direction and thereby establishes a dc plasma potential profile. These issues will be addressed in a future publication.

ACKNOWLEDGMENTS

We thank Dr. T. W. Johnston and Professor J. M. Dawson for many stimulating discussions.

This work was supported by University of California CALCOR program, Lawrence Livermore National Laboratory University research program and the U.S. Department of Energy.

APPENDIX: DERIVATION OF DISPERSION RELATIONS

In order to clarify the plasma parameter regions of the MSHI and the differences with other instabilities, we derive some well-known dispersion relations from Eq. (10) for several different plasma parameter regions. First, we show the density-potential relations for plasma electrons and ions.

1. Density-potential relations for electrons

Consider magnetized electrons ($\bar\omega^2\ll\Omega_e^2$). Equation (10) is reduced to

$$\frac{\tilde n_e}{n_{e0}}=-\frac{e\phi}{T_e}\left\{\frac{T_e}{m}\left(-\frac{k_y^2}{\Omega_e^2}+\frac{k_z^2}{\bar\omega^2+i\nu_e\bar\omega}-\frac{k_{ne}k_y}{\bar\omega\Omega_e}\right)\Big/\left(1-\frac{T_e}{m}\left[-\frac{k_y^2}{\Omega_e^2}+\frac{k_z^2}{\bar\omega^2+i\nu_e\bar\omega}-\frac{k_n^2}{\Omega_e^2}-\frac{k_{ne}k_y}{\bar\omega\Omega_e}\right]\right)\right\}. \tag{A1}$$

(1) When $T_e\simeq 0$, the second term in the denominator of Eq. (A1) is neglected. Together with $\nu_e\simeq 0$, we find

$$\frac{\tilde n_e}{n_{e0}}=\frac{e\phi}{m}\left(\frac{k_y^2}{\Omega_e^2}-\frac{k_z^2}{\bar\omega^2}+\frac{k_{ne}k_y}{\bar\omega\Omega_e}\right), \tag{A2}$$

where $\bar\omega=\omega-\omega_E$. (a) When $k_{ne}\simeq 0$, this reduces to

$$\frac{\tilde n_e}{n_{e0}}=\frac{e\phi}{m}\left(\frac{k_y^2}{\Omega_e^2}-\frac{k_z^2}{\bar\omega^2}\right). \tag{A3}$$

(b) When $k_z\simeq 0$, this reduces to

$$\frac{\tilde n_e}{n_{e0}}=\frac{e\phi}{m}\left(\frac{k_y^2}{\Omega_e^2}+\frac{k_{ne}k_y}{\bar\omega\Omega_e}\right). \tag{A4}$$

(2) When $T_e\neq 0$ and $c_e^2k_y^2\leqslant c_e^2k_n^2\ll\Omega_e^2$, we neglect the first term in the square bracket and the third term in the square bracket in the denominator in Eq. (A1)

$$\frac{\tilde n_e}{n_{e0}}=-\frac{e\phi}{T_e}\left\{\frac{T_e}{m}\left[\frac{k_z^2}{\bar\omega^2+i\nu_e\bar\omega}-\frac{k_{ne}k_y}{\bar\omega\Omega_e}\right]\Big/\left(1-\frac{T_e}{m}\left[\frac{k_z^2}{\bar\omega^2+i\nu_e\bar\omega}-\frac{k_{ne}k_y}{\bar\omega\Omega_e}\right]\right)\right\}, \tag{A5}$$

where $\bar\omega=\omega-\omega_E-\omega^*$. (a) When $\bar\omega/k_z\ll c_e$ and $\nu_e\simeq 0$, electrons can freely move along the B field and establish a thermodynamic equilibrium. Since the first term in the square bracket in Eq. (A5) is dominant, Eq. (A5) reduces to the Boltzmann relation

$$\frac{\tilde n_e}{n_{e0}}=\frac{e\phi}{T_e}. \tag{A6}$$

(b) When $\nu_e\simeq 0$ and $k_z\simeq 0$, we find the modified Boltzmann relation for the $k_z=0$ case

$$\frac{\tilde n_e}{n_{e0}}=\frac{e\phi}{T_e}\frac{\omega^*}{\omega-\omega_E}. \tag{A7}$$

(c) When $\nu_e\gg\bar\omega$ and $k_z\neq 0$, one finds the modified Boltzmann relation

$$\frac{\tilde n_e}{n_{e0}}=\frac{e\phi}{T_e}\frac{\omega^*+ik_z^2c_e^2/\nu_e}{\omega-\omega_E+ik_z^2c_e^2/\nu_e}. \tag{A8}$$

2. Density-potential relations for ions

When $T_i=0$, $\nu_i=0$ and $\mathbf{k}\cdot\mathbf{v}_{i0}\simeq 0$; Eq. (10) is reduced to

$$\frac{\tilde{n}_i}{n_{i0}}=\frac{e\phi}{T_e}\left(\frac{c_s^2k_y^2}{\omega^2-\Omega_i^2}+\frac{c_s^2k_z^2}{\omega^2}-\frac{c_s^2\Omega_ik_{ni}k_y/\omega}{\omega^2-\Omega_i^2}\right). \tag{A9}$$

(1) When ions are unmagnetized ($\omega\gg\Omega_i$), this reduces to

$$\frac{\tilde{n}_i}{n_{i0}}=\frac{e\phi}{T_e}\frac{c_s^2k^2}{\omega^2}. \tag{A10}$$

(2) When ions are weakly magnetized ($\omega\leqslant\Omega_i$) and $k_y\gg k_z,k_{ni}$, this reduces to

$$\frac{\tilde{n}_i}{n_{i0}}=\frac{e\phi}{T_e}\frac{c_s^2k_y^2}{\omega^2-\Omega_i^2}. \tag{A11}$$

(3) When ions are strongly magnetized ($\omega\ll\Omega_i$), this reduces to

$$\frac{\tilde{n}_i}{n_{i0}}=\frac{e\phi}{T_e}\left(-\frac{c_s^2k_y^2}{\Omega_i^2}+\frac{c_s^2k_z^2}{\omega^2}+\frac{\omega^*}{\omega}\right), \tag{A12}$$

where we assumed $k_{ni}=k_{ne}$. (a) When $k_z/k_y\gg\omega/\Omega_i$ or the ion Larmor radius for T_e is small ($b=c_s^2k_y^2/\Omega_i^2\ll1$), the first term on the right-hand side of Eq. (A12) is neglected and we find

$$\frac{\tilde{n}_i}{n_{i0}}=\frac{e\phi}{T_e}\left(\frac{c_s^2k_z^2}{\omega^2}+\frac{\omega^*}{\omega}\right). \tag{A13}$$

(b) When $k_z/k_y\ll\omega/\Omega_i$, we find

$$\frac{\tilde{n}_i}{n_{i0}}=\frac{e\phi}{T_e}\left(-\frac{c_s^2k_y^2}{\Omega_i^2}+\frac{\omega^*}{\omega}\right). \tag{A14}$$

3. Dispersion relations

Now by using the equations shown above together with the plasma approximation ($\tilde{n}_e=\tilde{n}_i$) or Poisson's equation, we derive well-known dispersion relations.

(1) When both electrons and ions are magnetized ($\omega\ll\Omega_i\ll\Omega_e$): (a) When the axial ion motion is important, and c_e is large enough to satisfy the Boltzmann relation for the electrons (even though $k_n\neq0$), Eqs. (A6) and (A13), together with the plasma approximation, give a dispersion relation for the collisionless drift wave[22]

$$\omega^2-\omega^*\omega-c_s^2k_z^2=0. \tag{A15}$$

(b) When electron collisions (electron–neutral or electron–ion collisions) are important while the ion axial motion is unimportant, the modified Boltzmann relation [Eq. (A8)] and Eq. (A14), together with the plasma approximation, give the dispersion relation for the collisional drift wave[11]

$$\omega^2+i\sigma_\parallel(\omega-\omega^*)=0, \tag{A16}$$

where $\sigma_\parallel=(k_z^2/k_y^2)(\Omega_e\Omega_i/\nu_e)$ and $b\ll1$ is assumed.

(2) When electrons are magnetized while ions are unmagnetized ($\Omega_i\ll\omega\ll\Omega_e$): (a) When $T_e\simeq0$ and electron collisions are unimportant; (i) when $k_{ne}\simeq0$, Eqs. (A3) and (A10) together with Poisson's equation give the modified two-stream instability;[2–4] (ii) when $k_z\simeq0$, Eqs. (A4) and (A10) give the flutelike drift instability.[1,3,5] (b) When $T_e\neq0$, $k_{ne}\neq0$; (i) when electron collisions are unimportant and $E_0=0$, Eqs. (A7) and (A10) give the stable antidrift mode[20]

$$\omega=\frac{c_s^2k^2}{\omega^*}; \tag{A17}$$

(ii) when electron collisions are important ($\omega\ll k_z^2c_e^2/\nu_e$) and $E_0=0$, Eqs. (A8) and (A10) give the ion-sound instability[22]

$$\omega\simeq c_sk\left(1+i\frac{\omega^*\nu_e}{2k_z^2c_e^2}\right). \tag{A18}$$

[1] Y. Kitagawa, T. Maekawa, and S. Tanaka, J. Phys. Soc. Jpn. **41**, 1041 (1976).
[2] M. Yamada and D. K. Owens, Phys. Rev. Lett. **38**, 1529 (1977).
[3] N. A. Krall and P. C. Liewer, Phys. Rev. A **4**, 2094 (1971).
[4] E. Ott, J. B. McBride, J. H. Orens, and J. P. Boris, Phys. Rev. Lett. **28**, 88 (1972).
[5] A. Hirose and I. Alexeff, Nucl. Fusion **12**, 315 (1972).
[6] A. Simon, Phys. Fluids **6**, 382 (1963).
[7] F. C. Hoh, Phys. Fluids **6**, 1184 (1963).
[8] K. I. Thomassen, Phys. Fluids **9**, 1836 (1966).
[9] S. C. Brown, *Basic Data of Plasma Physics* (MIT Press, Cambridge, MA, 1966).
[10] J. W. Sheldon, Phys. Rev. Lett. **8**, 64 (1962).
[11] F. F. Chen, *Introduction to Plasma Physics and Controlled Fusion*, 2nd ed. (Plenum, New York, 1984).
[12] F. F. Chen, in *Plasma Diagnostic Techniques*, edited by R. H. Huddlestone and S. L. Leonard (Academic, New York, 1965), Chap. 4.
[13] Y. Sakawa, C. Joshi, P. K. Kaw, V. K. Jain, T. W. Johnston, F. F. Chen, and J. M. Dawson, Phys. Rev. Lett. **69**, 85 (1992).
[14] Y. Sakawa, Ph.D thesis, University of California, Los Angeles, 1992.
[15] R. V. Aldridge and B. E. Keen, Plasma Phys. **12**, 1 (1970).
[16] As far as the Simon–Hoh instability mechanism is concerned, i.e., a space charge separation between the electron and ion density perturbations in the θ direction, the consequent perturbed azimuthal electric field $E_{\theta1}$ and the enhancement of the density perturbation by the $E_{\theta1}\times B_0$ drift, the beam term does not affect the instability.
[17] P. K. Kaw (private communication, 1991).
[18] S. Ichimaru, *Basic Principles of Plasma Physics* (Benjamin, Boston, MA, 1973).
[19] Equations (37) and (38) are identical to Eqs. (9) and (10), respectively in Ref. 5, since ω_{LH}, V_0, ω, and $K_n=(1/n_0)(dn_0/dx)$ in Ref. 5 are replaced by ω_{pi} (this is true when $\Omega_e\Omega_i\gg\omega_{pi}^2$), v_E, $\omega-kv_{0i}$, and $k_{nj}=|(1/n_{j0})(dn_{j0}/dx)|$ in Eq. (37), respectively.
[20] A. M. Fridman, Sov. Phys. Dokl. **9**, 75 (1964).
[21] The identical dispersion relation is given by Eq. (9) in Ref. 20 in the case when we apply the local approximation and $\nu_{ei}\simeq0$.
[22] B. B. Kadomtsev, *Plasma Turbulence* (Academic, New York, 1965).
[23] A. B. Mikhailovskii, Sov. Phys. JETP **16**, 364 (1963).